# Strong coupling in a single quantum dot–semiconductor microcavity system

**J. P. Reithmaier**[1], **G. Sęk**[1*], **A. Löffler**[1], **C. Hofmann**[1], **S. Kuhn**[1], **S. Reitzenstein**[1], **L. V. Keldysh**[2], **V. D. Kulakovskii**[3], **T. L. Reinecke**[4] **& A. Forchel**[1]

[1]*Technische Physik, Universität Würzburg, Am Hubland, D-97074 Würzburg, Germany*
[2]*Lebedev Physical Institute, Russian Academy of Science, 119991 Moscow, Russia*
[3]*Institute for Solid State Physics, Russian Academy of Science, 142432 Chernogolovka, Russia*
[4]*Naval Research Laboratory, Washington, DC 20375, USA*

* Permanent address: Institute of Physics, Wrocław University of Technology, 50-370 Wrocław, Poland

**Cavity quantum electrodynamics, a central research field in optics and solid-state physics[1–3], addresses properties of atom-like emitters in cavities and can be divided into a weak and a strong coupling regime. For weak coupling, the spontaneous emission can be enhanced or reduced compared with its vacuum level by tuning discrete cavity modes in and out of resonance with the emitter[2,4–13]. However, the most striking change of emission properties occurs when the conditions for strong coupling are fulfilled. In this case there is a change from the usual irreversible spontaneous emission to a reversible exchange of energy between the emitter and the cavity mode. This coherent coupling may provide a basis for future applications in quantum information processing or schemes for coherent control. Until now, strong coupling of individual two-level systems has been observed only for atoms in large cavities[14–17]. Here we report the observation of strong coupling of a single two-level solid-state system with a photon, as realized by a single quantum dot in a semiconductor microcavity. The strong coupling is manifest in photolumines-cence data that display anti-crossings between the quantum dot exciton and cavity-mode dispersion relations, characterized by a vacuum Rabi splitting of about 140 µeV.**

Strong coupling occurs when the emitter–photon interaction becomes larger than the combined atomic dipole decay rate and the cavity field decay rate. Then the irreversible spontaneous emission process of the emitter is replaced by a coherent periodic energy exchange between the emitter and the photon in the form of Rabi oscillations for timescales shorter than the inverse cavity field decay rate. In spectroscopic experiments this energy exchange results in anti-crossings between the atom-like emitter and cavity-mode dispersion relations and is characterized by the vacuum Rabi splitting. Solid state implementations, which would be highly desirable for future applications, for example in the area of quantum information processing[18–22], have not yet been achieved.

Semiconductor heterostructures are the best candidates for the observation of strong coupling in solids, because they permit the realization of solid state cavities in which atom-like emitters in the form of quantum dots (QDs) can be embedded. In these QD semiconductor cavities, strong and weak interaction can occur between the QD exciton (X) and discretized cavity (C) modes at a resonance ($E_X = E_C = E_0$). In a picture of coupled oscillators the energies of the interacting modes at resonance are[23,24]

$$E_{1,2} = E_0 - i(\gamma_C + \gamma_X)/4 \pm [g^2 - (\gamma_C - \gamma_X)^2/16]^{1/2} \quad (1)$$

where $\gamma_{C,X}$ is the full width at half maximum (FWHM) of the cavity and exciton modes, respectively, and $g$ is the exciton–photon coupling parameter. Strong coupling requires $g^2 > (\gamma_C - \gamma_X)^2/16$. This regime is characterized by a gap corresponding to the

vacuum Rabi splitting between the two energies $E_{1,2}$ on resonance. In contrast, for $g^2 \leq (\gamma_C - \gamma_X)^2/16$ the real parts of the energies $E_{1,2}$ are degenerate. This corresponds to the weak coupling case characterized, for example, by an enhancement of the spontaneous emission on resonance by the Purcell effect[2–3,5–7,25].

The exciton–photon coupling parameter $g$ is given by the scalar product of the transition matrix element of the QD exciton dipole moment with the local value of the electric field at the dot position. Assuming that the QD is located at the antinode of the electromag-netic field of the cavity mode, the coupling constant is related to the oscillator strength $f$ and the mode volume $V_m$ by[23]
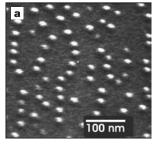
$$g = (\pi e^2 f)^{1/2}/(4\pi \varepsilon_r \varepsilon_0 m_0 V_m)^{1/2} \quad (2)$$

where $\varepsilon_r$ and $\varepsilon_0$ are the dielectric constants of cavity material and vacuum, respectively, and $m_0$ is the free electron mass. Equation (2) shows that $g$ depends on the QD exciton oscillator strength $f$ and on the mode volume $V_m$ as $(f/V_m)^{1/2}$.

$\gamma_C$ is related to the quality factor of the cavity $Q = E_C/\gamma_C$. The intrinsic value of the FWHM of the QD exciton $\gamma_X$ is on the order of a few µeV (ref. 26), which is much smaller than $\gamma_C$ ($\sim$100 µeV or larger in the present cavities; see Supplementary Information). The criterion for strong coupling can therefore be approximated by $g > \gamma_C/4$. This corresponds to the need to maximize the product $(f/V_m)^{1/2}Q$ so as to overcome the threshold for strong coupling. That is, one must realize QD excitons with large oscillator strength in high-$Q$ cavities with small mode volumes. In addition, because the coupling is given by the electromagnetic field strength at the exciton position, the QD should be located at the antinode of the field in all three dimensions (see Supplementary Information).

We have investigated strong coupling effects of a single QD with discrete cavity modes in a semiconductor micropillar cavity. Details of the structure are given in the Supplementary Information. The epitaxial structures provide strong optical confinement in the growth direction by Bragg reflector stacks composed of 20 and 23 periods of GaAs and AlAs layers in the top and bottom mirrors surrounding a GaAs cavity. At the centre of the GaAs cavity at the antinode of the fundamental mode in growth direction an InGaAs QD layer is embedded.

As discussed above, one has to maximize the oscillator strength of the QD exciton as well as the cavity quality factor $Q$ at small mode volume $V_m$ so as to reach strong coupling for single QDs. The oscillator strength of the QD excitons increases with the dot size. It has therefore been suggested[23] that large ('natural') QDs be used,
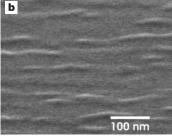


**Figure 1** Scanning electron micrographs of InGaAs QDs with different In contents before overgrowth. The samples have been tilted with respect to the electron beam direction. The magnification along the vertical axis is therefore about one-third of that along the horizontal direction. **a**, For an indium content of 60%, typical self-assembled dots are formed owing to the large lattice mismatch to the GaAs substrate accompanied by a large resulting strain. These QDs have a characteristic diameter of 15–20 nm. **b**, Much larger dots are formed for an In content of 30%, as used in the present micropillars. These dots are usually elongated with lengths on the order of 100 nm or larger and widths of about 30 nm. The larger size gives rise to an increase in the excitonic oscillator strength compared with the smaller self-assembled dots.

which can be obtained by growth fluctuations of quantum wells instead of small self-assembled dots. For the present work we have realized $In_{0.3}Ga_{0.7}As$ natural dots. As shown by the scanning electron micrographs in Fig. 1, the use of 30% In results in large asymmetric dots with typical lengths of 100 nm and widths of about 30 nm. Conventional self-assembled dots shown in Fig. 1 for an In content of 60% are characterized by a more symmetric shape and diameters of 15–20 nm. By using natural dots with 30% In content the dot area can therefore be increased by about an order of magnitude, which should result in a significant enhancement of the oscillator strength.

Photoluminescence spectroscopy on the as-grown sample shows a sharp cavity emission with $Q$ factors of about 12,000. By removing the upper Bragg reflector the emission of the QD layer can be studied without cavity effects. At low temperature (4 K to about 50 K) the QD layer exhibits a broad photoluminescence spectrum in the energy range 1.33–1.35 eV because of inhomogeneous broadening due to fluctuations in QD size.

To obtain high-$Q$ cavities with small mode volumes as required for the observation of strong coupling effects, we have fabricated micropillars of various sizes from the epitaxial samples. Micropillars with circular cross-sections (diameters from 0.5 to 4 μm) have been processed by electron-beam lithography and reactive ion-etching in an inductively coupled $Ar/Cl_2$ plasma. Figure 2a shows such a micropillar with a diameter of 800 nm and a height of about 6 μm. The combination of a high-$Q$ epitaxial cavity with optimized micropillar processing allows us to realize micropillars with $Q$ factors of 8,000–9,000 for 2 μm diameter, 7,000–9,000 for 1.5 μm diameter and 2,000–4,000 for 1.0 μm diameter.

For cylindrical micropillars with constant cavity height and different pillar diameters the need to maximize $(f/V_m)^{1/2}Q$ for the observation of strong coupling corresponds to the maximization of $Q/d_C$ at a given oscillator strength $f$. Here $d_C$ denotes the diameter of the pillars. For cavities with diameters of 2, 1.5 and 1.0 μm and $Q$ factors at the centre of the ranges given above, we obtain values of 4,250, 5,300 and 3,000 μm$^{-1}$ for $Q/d_C$, respectively. This implies

that the 1.5-μm diameter micropillars offer the best conditions for the observation of strong coupling.

For single-dot photoluminescence studies, samples with micropillars 1.5 μm in diameter were mounted in a variable-temperature cryostat of a microphotoluminescence set-up. Luminescence of single dots in individual pillars is spectrally resolved by a 1-m double spectrometer equipped with a nitrogen-cooled charge-coupled-device camera. The spectral resolution of the system amounts to about 50 μeV. For optical excitation the beam of a frequency-doubled continuous-wave Nd:YAG laser at 532 nm was focused into a spot 3 μm in diameter centred at the pillar by a microscope objective, which was also used to collect the emission of the sample.

Figure 2b shows a photoluminescence spectrum of one of the 1.5-μm-diameter pillars. The spectrum is dominated by the emission of the cavity mode located at 1.316 eV. The optical mode has a FWHM of 0.15 meV, corresponding to a $Q$ factor of 8,800. In the high-$Q$ cavities investigated here, the emission of the individual dots results in lines of lower intensity and smaller FWHM. The observed FWHM of the single-dot lines located outside the interaction range with the cavity mode indicates the spectral resolution of the experiment.

To investigate the coupling between the cavity mode and individual QDs, the energies of both must to be tuned through each other. For tuning through resonance, the different temperature variations of the bandgap and of the refractive index $n$ are used. The temperature dependence of the emission energy of the QD excitons (typically $-0.04$ meV K$^{-1}$ at 25 K) is governed by the temperature dependence of the bandgap, whereas the temperature dependence of the cavity modes (about $-0.005$ meV K$^{-1}$ at 25 K) is determined by the much weaker temperature dependence of the refractive index. By selecting micropillars with single-QD exciton emissions near to the energy of the cavity resonance it is possible to tune the excitations in and out of resonance.

Figure 3 shows spectra taken from a microcavity 1.5 μm in diameter at different temperatures between 5 and 30 K. At 5 K the emission consists of the cavity mode C centred at about 1.32335 eV and a QD exciton X emission at slightly higher energy (1.32365 eV). By using lineshape fits of the 5 K spectrum with two lorentzians, we find that the emission intensity of the dot exciton is smaller by about one order of magnitude than that of the cavity mode. The FWHM of the cavity mode (180 μeV for low-excitation conditions) is found to be larger by about 2.5-fold than the FWHM of the dot. For
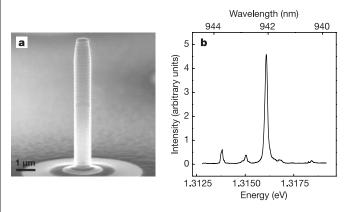


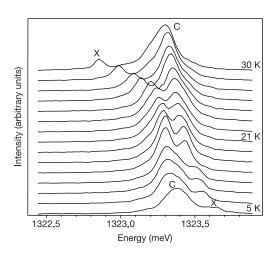**Figure 2** Scanning electron micrograph and photoluminescence of processed microcavity pillars. **a**, Scanning electron micrograph of a pillar with a diameter of about 0.8 μm. By a combination of electron-beam lithography and reactive dry etching, micropillars with close to vertical and defect-free sidewalls are obtained, as required for high-$Q$ cavities. **b**, Microphotoluminescence spectrum for a 1.5-μm diameter microcavity ($Q = 8,800$) with $In_{0.30}Ga_{0.70}As$ QDs recorded at 5 K. A few sharp (spectral-resolution-limited linewidths) peaks related to the emission from QDs and a strong and wider peak connected to the fundamental cavity mode are observed. Even without a dot on resonance, there is cavity emission due to population through, for example, phonon-assisted scattering from the dot ensemble in the pillar. The cavity peak is particularly pronounced owing to the high $Q$ factors of the present structures. QD lines that show, at low temperature, energies slightly higher than that of the cavity mode can be temperature tuned through the cavity resonance.



**Figure 3** Temperature dependence of photoluminescence spectra for a 1.5-μm microcavity ($Q = 7,350$) showing the tuning of a single QD exciton through resonance with the cavity mode. A clear anti-crossing is observed owing to strong coupling between the QD exciton and the microcavity photon mode.

increasing temperature up to 30 K the emission consists of two distinct features. However, at 30 K the components of the emission have exchanged their properties: now the low-energy line has an emission intensity and FWHM similar to that of the line located at 5 K at higher energy and therefore has to be assigned to the QD exciton. Simultaneously, the high-energy line displays an emission intensity and FWHM that correspond to the values for the cavity mode at 5 K. Over the entire temperature range the energies of the two contributions to the spectrum are well separated and avoid crossing each other. All the above findings are clear indications for an anti-crossing of the single QD exciton and cavity-mode dispersions due to strong coupling between those modes.

Figure 4 shows experimentally observed variations of the energies, FWHMs and intensities of the coupled modes for varying temperature for two 1.5 µm micropillars exhibiting strong and weak coupling, respectively. The data are plotted against the change of the energies of a different, non-interacting QD in the same cavity that is separated by about 5 meV from the cavity-mode position. The origin of this energy scale has been placed at the resonance.
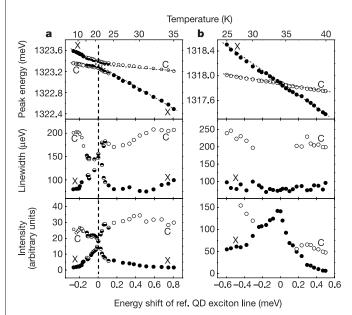


**Figure 4** Dependences of photoluminescence peak energies, linewidths and integrated intensities on the temperature-generated energy shift of a reference QD for strong and weak coupling. The reference QD-related peak is located about 5 meV above the cavity mode and does not interact with the cavity (bottom scale). At the top is the temperature axis (nonlinear). All data have been obtained by fits of lorentzian lineshapes to the experimental spectra. **a**, Data for a single dot–cavity system in strong coupling. C (open dots), cavity-mode data; X (filled dots), QD exciton data; partly filled dots, data on or near resonance, where the strong coupling results in coupled modes. Top, anti-crossing of QD exciton and cavity mode. Centre, variation of exciton, cavity and coupled-mode FWHM linewidths during anti-crossing. Bottom, exchange of intensities of single-dot exciton and cavity mode (integrated over the respective lorentzian used for the fits) resulting from anti-crossing. **b**, Experimental results for a dot–cavity system in the weak coupling regime. Top, crossing of cavity (C, open dots) and single QD exciton (X, filled dots) dispersions. Centre, variation of single-dot exciton FWHM linewidths during crossing of the dispersions (open circles). Values for the cavity mode are shown only above and below the resonance, because a reliable determination of the cavity FWHM on resonance is prevented by the small cavity contribution. Bottom, variation of integrated single-dot exciton and cavity-mode intensities. The dot intensity on resonance shows a clear peak due to the Purcell effect. In comparison with those in **a**, the experiments shown in **b** were performed at elevated temperatures between 25 and 40 K. Because of increasing thermal ionization, the plot of intensity against detuning shows a decrease in QD emission intensity superimposed on the Purcell effect peak.

As plotted in the top panel of Fig. 4a for a strongly coupled system, the energies of the higher-lying mode show a fairly strong variation before reaching the resonance (below about 20 K), which changes to a much weaker dependence. Simultaneously the low-energy mode, which displays only a weak temperature variation at low temperature, changes to a stronger temperature dependence above 20 K. The top panel of Fig. 4b shows experimental data for the energy variation of both modes for a micropillar with dot exciton and cavity mode in a weak coupling situation during temperature tuning. In striking contrast to the strong coupling case shown in Fig. 4a, the exciton dispersion with its steep characteristic temperature dependence crosses the weakly temperature-dependent cavity mode without any indication of a gap. By comparing the temperature dependences of the strongly coupled modes in Fig. 4a with the temperature variations of weakly interacting QD excitons and cavity modes in Fig. 4b, we observe that weakly interacting excitons have similar temperature dependences to the steep sections of the dispersions of the coupled modes. The less temperature dependent sections of the coupled mode dispersions correspond to the temperature variations of uncoupled cavity modes. For the upper branch the anti-crossing results in a change from an exciton-like dispersion to a cavity-mode-like one, whereas the lower branch changes from a cavity-mode dispersion to that of an exciton with increasing temperature.

As shown in the top panel of Fig. 4a for the case of strong coupling, the energy separation of the coupled modes on resonance amounts to about 140 µeV. This corresponds to the vacuum Rabi splitting of this coupled single two-level emitter (QD exciton) solid state cavity system. Using equation (1) and the experimental values for the FWHM of the cavity mode out of resonance and the observed splitting, we estimate a value of $g \approx 0.08$ meV for the coupling constant. The threshold for the onset of strong coupling, which is given by a vanishing square root term in equation (1), corresponds to $g = 0.045$ meV.

By numerical calculations we obtain mode volumes of about $0.3\,\mu\mathrm{m}^3$ for the present micropillar cavities. Using this value and equation (2) we estimate the effective oscillator strength to about 50. This value is about fourfold higher than those reported for self-assembled InAs QDs[23]. However, it agrees with values observed for natural QDs in the GaAs/AlGaAs system[27]. The use of dots with large oscillator strengths is crucial for the observation of strong coupling: from equation (1), for the present $Q/d_C$ values and small self-assembled InAs dots with an oscillator strength of about 10, the QD–cavity system would still be in the weak coupling regime.

In the middle and bottom panels of Fig. 4 the variations of the linewidths (FWHM) and intensities of the cavity–dot system for the cases of strong and weak coupling are compared with each other. For strong coupling we observe an exchange of linewidths and intensities at the anti-crossing (Fig. 4a). As a result of the anti-crossing, both contributions to the emission can be analysed reliably over the entire temperature range. Because of the absence of a gap in the weak coupling regime, the analysis of the individual FWHMs and intensities of the two components is more complex than for the strong coupling case (see Supplementary Fig. 2). We therefore include only those features in Fig. 4b that can be evaluated reliably. These are the emission intensity and FWHM of the QD exciton. For the weak coupling, the emission intensity of the dot increases strongly on resonance owing to the Purcell effect[4–9,25]. Within experimental accuracy we find no broadening for the dot line due to interaction with the cavity mode.

The present results for strong coupling are due to the coherent interaction of a single QD emitter with a single photon. As described in the Supplementary Information there is no indication for the contribution of two dots when the dots are far from resonance. Because the oscillator strength derived from our experiment also agrees with values for excitons in single QDs, we conclude that there is only one dot participating in the strong

# letters to nature

coupling. The excitation power used in the strong coupling experiments of $2\,\mu W$ corresponds to $1.5 \times 10^9$ photons s$^{-1}$ in the cavity averaged over time; that is, interactions of the single QD with multiple photons can be neglected.

Our experiments demonstrate that long-sought solid state implementations of the strongly coupled cavity-mode–two-level-emitter systems are feasible by using single QDs in high-$Q$ cavities with small mode volumes. With further improvements, for example using higher-$Q$ cavities or QDs placed at the in-plane mode centre, these systems have the potential for wide application ranging from nonlinear optics[28] to quantum information processing[18–22].

1. Yamamoto, Y. & Slusher, R. E. Optical processes in microcavities. *Physics Today* **46,** 66–73 (1993).
2. Gerard, J. M. & Gayral, B. InAs quantum dots: artificial atoms for solid-state cavity-quantum electrodynamics. *Physica E* **9,** 131–139 (2001).
3. Vahala, K. J. Optical microcavities. *Nature* **424,** 839–846 (2003).
4. Kleppner, D. Inhibited spontaneous emission. *Phys. Rev. Lett.* **47,** 233–236 (1981).
5. Goy, P., Raimond, J. M., Cross, M. M. & Haroche, S. Observation of cavity-enhanced single-atom spontaneous emission. *Phys. Rev. Lett.* **50,** 1903–1906 (1983).
6. Gabrielse, G. & Dehmelt, H. Observation of inhibited spontaneous emission. *Phys. Rev. Lett.* **55,** 67–70 (1985).
7. Hulet, R. G., Hilfer, E. S. & Kleppner, D. Inhibited spontaneous emission by a Rydberg atom. *Phys. Rev. Lett.* **55,** 2137–2140 (1985).
8. Gerard, J. M. *et al.* Enhanced spontaneous emission by quantum boxes in a monolithic optical microcavity. *Phys. Rev. Lett.* **81,** 1110–1113 (1998).
9. Bayer, M. *et al.* Inhibition and enhancement of the spontaneous emission of quantum dots in structured microresonators. *Phys. Rev. Lett.* **86,** 3168–3171 (2001).
10. Solomon, G. S., Pelton, M. & Yamamoto, Y. Single-mode spontaneous emission from a single quantum dot in a three-dimensional microcavity. *Phys. Rev. Lett.* **86,** 3903–3906 (2001).
11. Pelton, M. *et al.* Efficient source of single photons: a single quantum dot in a micropost microcavity. *Phys. Rev. Lett.* **89,** 233602-1-4 (2002).
12. Santori, C., Fattal, D., Vuckovic, J., Solomon, G. S. & Yamamoto, Y. Indistinguishable photons from a single-photon device. *Nature* **419,** 594–597 (2002).
13. Michler, P. *et al.* A quantum dot single-photon turnstile device. *Science* **290,** 2282–2285 (2000).
14. Hood, C. J., Chapman, M. S., Lynn, T. W. & Kimble, H. J. Real-time cavity QED with single atoms. *Phys. Rev. Lett.* **80,** 4157–4160 (1998).
15. Mabuchi, H. & Doherty, A. C. Cavity quantum electrodynamics: coherence in context. *Science* **298,** 1372–1377 (2002).
16. McKeever, J. *et al.* Experimental realization of one-atom laser in the regime of strong coupling. *Nature* **425,** 268–271 (2003).
17. McKeever, J. *et al.* State-insensitive cooling and trapping of single atoms in an optical cavity. *Phys. Rev. Lett.* **90,** 133602-1-4 (2003).
18. Monroe, C. Quantum information processing with atoms and photons. *Nature* **416,** 238–246 (2002).
19. Imamoglu, A. *et al.* Quantum information processing using quantum dot spins and cavity QED. *Phys. Rev. Lett.* **83,** 4204–4207 (1999).
20. Stievater, T. H. *et al.* Rabi oscillations of excitons in single quantum dots. *Phys. Rev. Lett.* **87,** 133603-1-4 (2001).
21. Li, X. Q. & Yan, Y. J. Quantum computation with coupled quantum dots in optical microcavities. *Phys. Rev. B* **65,** 205301-1-5 (2002).
22. Kiraz, A., Atatüre, M. & Imamoglu, A. Quantum-dot single-photon sources: Prospects for applications in linear optics quantum-information processing. *Phys. Rev. A.* **69,** 032305 (2004).
23. Andreani, L., Panzarini, G. & Gerard, J. M. Strong-coupling regime for quantum boxes in pillar microcavities: Theory. *Phys. Rev. B* **60,** 13276–13279 (1999).
24. Rudin, S. & Reinecke, T. L. Oscillator model for vacuum Rabi splitting in microcavities. *Phys. Rev. B* **59,** 10227–10233 (1999).
25. Purcell, E. M. Spontaneous emission probabilities at radio frequencies. *Phys. Rev.* **69,** 681 (1946).
26. Bayer, M. & Forchel, A. Temperature dependence of the exciton homogeneous linewidths in In$_{0.6}$Ga$_{0.4}$As/GaAs self-assembled quantum dots. *Phys. Rev. B* **65,** 041308-1-4 (R) (2002).
27. Guest, J. R. *et al.* Measurement of optical absorption by a single quantum dot exciton. *Phys. Rev. B* **65,** 241310-1-4 (2002).
28. Shimizu, Y. *et al.* Control of light pulse propagation with only a few cold atoms in a high finesse microcavity. *Phys. Rev. Lett.* **89,** 233001-1-4 (2002).

**Correspondence** and requests for materials should be addressed to A.F. (alfred.forchel@physik.uni-wuerzburg.de).

---

# Vacuum Rabi splitting with a single quantum dot in a photonic crystal nanocavity

**T. Yoshie**[1], **A. Scherer**[1], **J. Hendrickson**[2], **G. Khitrova**[2], **H. M. Gibbs**[2], **G. Rupper**[2], **C. Ell**[2], **O. B. Shchekin**[3] & **D. G. Deppe**[3]

[1]*Electrical Engineering, California Institute of Technology, Pasadena, California 91125, USA*
[2]*Optical Sciences Center, The University of Arizona, Tucson, Arizona 85721, USA*
[3]*Microelectronics Research Center, Department of Electrical and Computer Engineering, The University of Texas at Austin, Austin, Texas 78712, USA*

·······························································

**Cavity quantum electrodynamics (QED) systems allow the study of a variety of fundamental quantum-optics phenomena, such as entanglement, quantum decoherence and the quantum–classical boundary[1–9]. Such systems also provide test beds for quantum information science. Nearly all strongly coupled cavity QED experiments have used a single atom in a high-quality-factor (high-$Q$) cavity. Here we report the experimental realization of a strongly coupled system in the solid state: a single quantum dot embedded in the spacer of a nanocavity, showing vacuum-field Rabi splitting exceeding the decoherence linewidths of both the nanocavity and the quantum dot. This requires a small-volume cavity and an atomic-like two-level system[5,10]. The photonic crystal[11] slab nanocavity—which traps photons when a defect is introduced inside the two-dimensional photonic bandgap by leaving out one or more holes[12]—has both high $Q$ and small modal volume $V$, as required for strong light–matter interactions[13]. The quantum dot has two discrete energy levels with a transition dipole moment much larger than that of an atom[14–16], and it is fixed in the nanocavity during growth.**

The study of vacuum Rabi splitting has been an exciting subfield of atomic physics since its first observation with many atoms in the early 1980s; see ref. 1 for a history of the field. After a decade of gradually improving the $Q$ of the cavity and decreasing its volume, vacuum Rabi splitting was seen with a single atom. This opened exciting opportunities for the field of atomic cavity QED, and many experiments followed[1–7]. For such a truly quantum system, the optical properties are changed by the addition of a single photon or single atom, and the quantum–classical boundary can be studied[2–4]. But because atoms can move and even escape, their coupling is time-dependent; clearly, the next goal was to localize a cold atom inside the cavity using atomic traps[6].

In the field of semiconductors, 12 years elapsed between seeing non-perturbative normal mode coupling[17], analogous to many-atom vacuum Rabi splitting[10], and the observation of strong coupling between a single quantum dot (SQD) and a small-volume crystal nanocavity. This advance, which produced opportunities for truly quantum-optics cavity QED experiments in semiconductors, owes much to the extensive studies of (and improvements in) SQDs and monolithic cavities. The semiconductor approximation to a two-level system is a SQD, a small semiconductor crystal confined in three dimensions by a higher-bandgap material[14–16]. The sharp emission lines observed from submicrometre collection spots were shown to arise from transitions between discrete energy levels of the quantum dot (QD) depending upon size and shape[18,19]. Coherent transient experiments were performed on these atom-like transitions[16,20], and their spontaneous emission was enhanced[21–23] and inhibited[22] by the Purcell effect within microcavities[24] of higher and higher $Q$. The transitions of a SQD can be separated enough for the lowest transition to exhibit anti-bunching, and cavity enhanced spontaneous emission can lead to one photon on demand into a desired mode[21,25].